Journal of Science: Advanced Materials and Devices 3 (2018) 366–370

Contents lists available at ScienceDirect

Journal of Science: Advanced Materials and Devices

journal homepage: www.elsevier.com/locate/jsamd

Original Article

Linear and non-linear electrical behaviors in graphene ribbon based devices

Rachid Fates [a, b, *], Jean-Pierre Raskin [b]

[a] Electronic Department, LEM Laboratory, Université de Jijel, B.P. 98, Ouled Aissa, 18000, Jijel, Algeria
[b] Institute of Information and Communication Technologies, Electronics and Applied Mathematics, Université catholique de Louvain, Place du Levant, 3, B-1348, Louvain-la-Neuve, Belgium

A R T I C L E I N F O

Article history:
Received 21 March 2018
Received in revised form
30 May 2018
Accepted 2 June 2018
Available online 15 June 2018

Keywords:
Graphene monolayer
Electrical properties
Linear behavior
Nonlinear behavior

A B S T R A C T

We experimentally investigate the carrier transport in back-gated graphene ribbons. The ribbons are monolayer graphene formed by the chemical vapor deposition process and transferred on the SiO_2/Si substrate. Electrical measurements show that two categories of electrical behavior are distinguished, respectively, linear and nonlinear. The *in-situ* Raman characterization along the ribbon area highlights interesting results for the 2D peaks shift. The Raman shift variation corresponding to the position of the 2D peaks between all measured spectra extends from 2697 cm^{-1} to 2700 cm^{-1} for devices exhibiting a linear behavior. While, for the devices exhibiting a nonlinear behavior, the variation range is more important, from 2686 cm^{-1} to 2704 cm^{-1}. These results reveal that the carrier density is non-uniform and localized in term of concentration over the ribbon area, and the electrical behavior appears to be strongly related to the graphene local carrier density.

1. Introduction

From the isolation of real two-dimensional carbon sheet in 2004 [1], the discovery of graphene has enabled intense fundamental and applied research activities in this novel two-dimensional carbon based electronic system. The huge scientific and technological interest in graphene has been largely driven by its physical properties, that make graphene as material with interesting low-dimensional physics and potential applications in electronics [2–5]. From electronic device point of view, graphene is a promising material for future smaller and faster electronics, it has been suggested as a channel material for the next generation of field effect transistors (FETs), and as a semi/conductive sheet upon which nanometer scale devices may be patterned to create single electron or few electron transistors [6].

The physical properties of graphene are the most explored ones for the new fundamental scientific perspectives [7]. Several studies used Raman spectroscopy to analyze the carrier density over large area of the samples [8–11]. This nondestructive characterization technique can be used as a support to explain the carrier density influence on electron transport.

Nonlinear electrical behavior was already reported for monolayer graphene ribbons at critical cryogenic temperature [12]. The nonlinear electrical behavior at the cryogenic temperature in the current–voltage characteristics (or I_{ds}–V_{ds} curves) is attributed to the presence of an energy gap in graphene monolayer acting as a potential barrier for the carriers. Shin et al. [13] reported that the nonlinear electrical behavior in graphene ribbons was caused by doping in the ribbons. This conclusion was drawn after making measurements in two steps: first measurements were nonlinear, after performing a thermal treatment generated by a high current annealing on their devices, the nonlinear behavior were never been observed with more than 20 devices and the curves had a linear shape. They concluded that the nonlinear phenomenon is strongly correlated to electrochemical reactions caused by active radicals which are attached and detached to the graphene channel from air.

For the graphene ribbon based devices, many papers investigate the electrical behavior of the metal/graphene contact [7,14–16] since of its importance for the graphene FET applications. Experimental investigation [15] reported that the doped monolayer graphene beyond ~10^{13} cm^{-2} produces an ohmic behavior in

* Corresponding author. Electronic Department, LEM Laboratory, Université de Jijel, B.P. 98, Ouled Aissa, 18000, Jijel, Algeria.
E-mail addresses: rachid.fates@yahoo.fr, rachid.fates@student.uclouvain.be (R. Fates).
Peer review under responsibility of Vietnam National University, Hanoi.

https://doi.org/10.1016/j.jsamd.2018.06.001

contacting metal. In addition, in terms of theory and modeling of the graphene devices [17–21], it is important to get an ohmic graphene/metal contact in order to study the electronic behavior of the graphene as an active material in FET devices. In this emergent field of research, previous study of Vicarelli et al. [22] reported the importance of the graphene quality and the graphene defects on the optimization of the electrical properties of graphene devices.

In our study, hundreds of devices have been fabricated and measured. We observed two typical electrical behaviors: linear and non-linear output characteristics.

The objective of this work is the highlighting of the non-uniform carrier concentration impact on graphene ribbons electrical behavior. First, the scanning electron microscopy (SEM) characterizations show the studied devices. We will in parallel expose outlines of the devices fabrication process and the experimental setup for electrical measurements. Second, we present the typical electrical behaviors for hundreds measured devices. Then, the Raman characterization is used to evaluate the carrier's concentration in the graphene ribbon, leading to original conclusion.

2. Experimental

Two-terminal back-gated monolayer graphene ribbon devices are fabricated on conventional silicon (Si) substrate covered by a 90 nm-thick thermal silicon dioxide (SiO_2). Chemical vapor deposition (CVD) process is used for single-layer graphene deposition on Copper in CVD furnace, then the graphene layer is transferred on the SiO_2/Si substrate. The quality of graphene is checked with optical microscopy, SEM, Raman spectroscopy and Hall measurements. The large area Hall measurements reveal initial doping concentration of 1.9×10^{13} cm^{-2} and a mobility of 410 cm^2/V. For the devices fabrication, optical lithography is used for electrode patterning through a mask, an ohmic Ti/Au (10 nm/100 nm) metallic contacts are deposited by thermal evaporation and defined with lift-off technique.

After the fabrication step, it was necessary to evaluate the quality to select the best wafer for the measurements. For that, Raman spectroscopy was performed on the different samples. Even though SEM imaging provides a more precise view of the graphene, this technique was used only on few devices because it is known to induce a contamination of the graphene surface. During these steps the rest of the devices were kept in a nitrogen atmosphere enclosure.

In order to study the electrical behavior in the graphene ribbons, we performed measurements in the vacuum on hundreds of devices. The devices are 10 μm-long by 16 μm-wide supported by the SiO_2/Si substrate. In Fig. 1, one of the measured devices is illustrated. The three dimensional (3D) view of the device structure is shown in Fig. 1a. The graphene ribbon between the source and drain metallic contacts can be distinguished on SEM image in Fig. 1b. The typical Raman spectrum of the graphene on SiO_2 is shown in Fig. 1c. The 2D peak is fitted by one single Lorentzian component indicating that the graphene ribbon is monolayer. Complementary information about the Raman measurements is given in Section 3.2.

The electrical measurements of the graphene ribbons at room temperature were tested using a micro probe station (CPX Cryogenic 6 probes system) under vacuum with chamber pressure below 10^{-5} mTorr, reached with a turbo vacuum pump. The samples were kept under vacuum for 6 h for the test, and one day before the measurements, to minimize any effect resulting from any adsorbed or desorbed particles or radicals on the surface of graphene. The current–voltage data were collected thereafter by an Agilent K4200-SCS semiconductor analyzer. The 3D schematic view of the measurement setup is shown in Fig. 2g.

3. Results and discussion

3.1. Electrical characterization

From all the measured devices, we distinguish two typical electrical behaviors that can illustrate all the devices. First, we note the nonlinear (NL) device: the measurements presenting a NL behavior, second, the linear (L) device: the measurements presenting a L behavior, as shown in Fig. 2. As reported previously [13], we also make measurements on our devices before and after a high current annealing in order to generate a thermal heating in the graphene ribbons. None difference was observed in the measurements with respect to those presented in Fig. 2.

From Fig. 2a and b, while the gate voltage is varied from 0 V to 40 V, the resistance of the device increases monotonically, this evolution indicates that the ribbons are of p-type. In Fig. 2c–f, we compare the room temperature output characteristics for each gate voltage value. The comparison between the two behaviors for a constant back gate voltage shows that there is a difference in current transport behavior in the ribbon for both NL and L devices.

We can easily differentiate two slopes from the NL output characteristics. A first slope at low drain voltage, for $V_{ds} < 0.8$ V, defining a linear low voltage regime. The second slope have a larger tilt, for $V_{ds} > 0.8$ V, shows a kink effect, defining a high voltage regime.

In Fig. 3a, the drain current decreases with increasing back gate voltage down to reach a minimum value corresponding to the charge neutrality point (CNP) at $V_{gs} = 39$ V. From these data, we can define the minimum carrier concentration $n_{min} = 4 \times 10^{12}$ cm^{-2} and the mobility $\mu = 560$ cm^2/V of the graphene. This result demonstrates the influence of the gate voltage on the graphene ambipolar behavior.

From the L device measurements shown in Fig. 3b, it is clear that the CNP is situated beyond 60 V. The ribbon cannot resist to such voltage range, so, we cannot define the CNP with accuracy. However, the comparison of these measurements with those in Fig. 3a reveals that the L device is more doped than NL device. Consequently, these results suggest that the difference in both electrical behaviors is directly related to the position of the CNP, i.e., related to the graphene carrier's concentration. For more accuracy, we used Raman analysis to evaluate the carrier's concentrations over the graphene ribbons.

Otherwise, in term of experimental measurements, all devices having a CNP > 60 V exhibit a linear behavior, while, all devices exhibiting a nonlinear behavior have a CNP in a range from 39 V to 55 V.

3.2. Raman characterization

In this part, we aim to identify how the Raman shift changes through the ribbon area. We investigate the NL and L ribbons with Raman spectroscopy with 514.5 nm laser excitation wavelength and 1% power filter in order to do not damage the graphene. The Raman spectra are collected with a ×100 objective, the spectrometer with 2400 line/mm grating and the Raman resolution is 0.2 cm^{-1}. Changes in the bands position are reported.

As shown in Fig. 2, the nonlinear behavior is independent of the back gate voltage, so, the Raman measurements were performed without any bias.

The influence of the graphene carrier's concentration on Raman spectra was already studied, it was demonstrated that Raman spectroscopy is an excellent method to estimate the carrier's concentration in graphene [8–11]. According to Ferrari et al. [8], the 2D peak is independent of the defects, thus, it is always present. Moreover, the shape of the 2D peak is the most effective way to

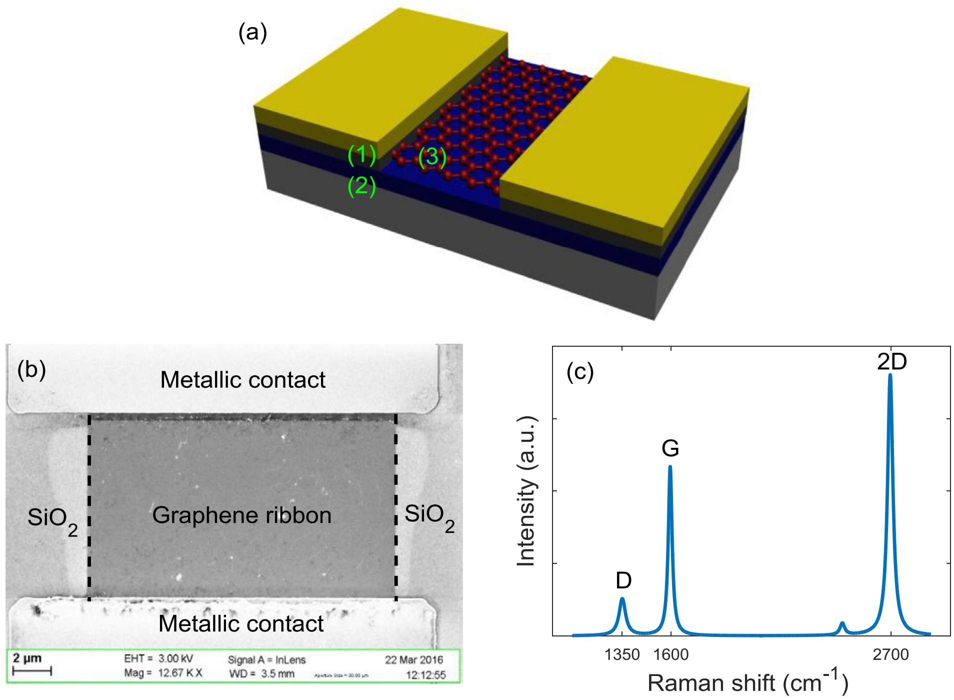

Fig. 1. (a) 3D perspective view of the devices structure, (1) Au/Ti metallic contact, (2) SiO_2/Si substrate, (3) graphene ribbon. (b) SEM image of one graphene ribbon device, analyzed with InLens electron detector. (c) Raman spectrum of the graphene ribbon showing D, G, 2D peaks.

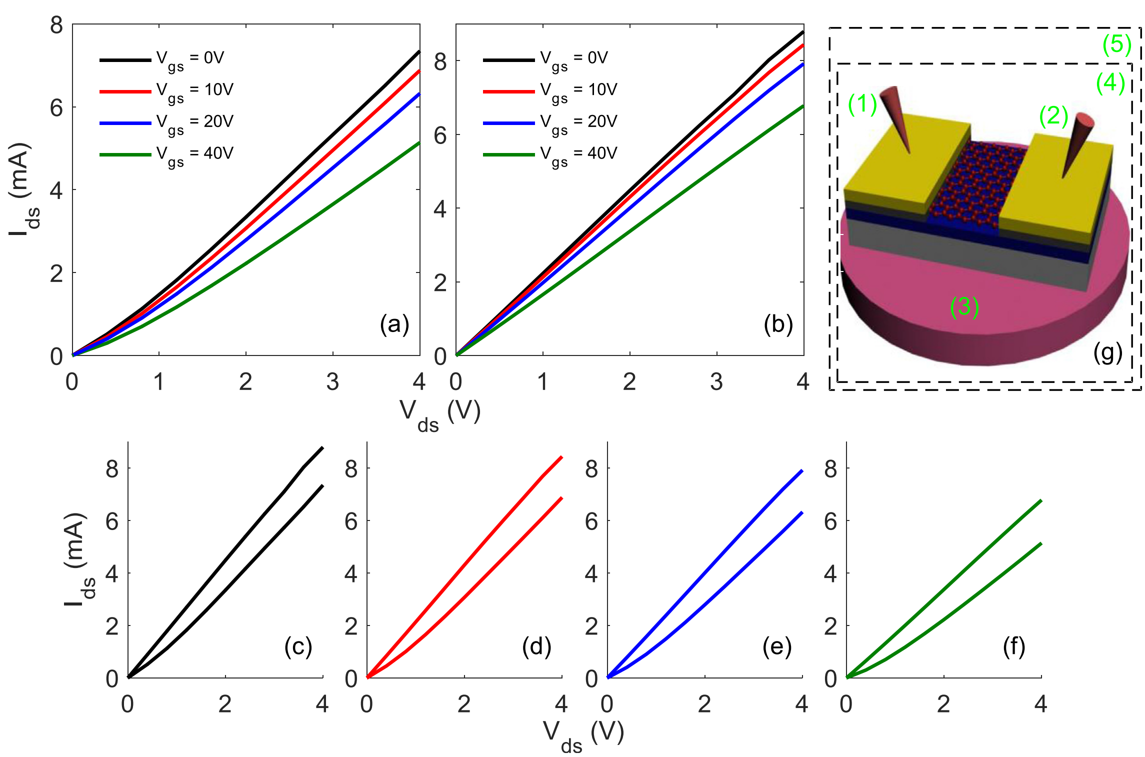

Fig. 2. Output characteristics measurements showing the (a) non-linear (NL) and (b) linear (L) electrical behaviors. Comparison between both NL and L electrical behaviors for (c) $V_{gs} = 0$ V, (d) $V_{gs} = 10$ V, (e) $V_{gs} = 20$ V and (f) $V_{gs} = 40$ V. (g) 3D schematic representation of the measurements setup with: (1) source probe, (2) drain probe, (3) sample stage as back gate probe, (4) thermal chamber and (5) vacuum chamber.

identify the single layer of the graphene domains. For these reasons, we performed the Raman measurements on the investigated NL and L devices especially on 2D peak in order to define the variation of the band positions across the ribbons area. The measurement details are summarized in Fig. 4.

In Fig. 4a, the corresponding 2D peak positions for the L device are illustrated. We can distinguish a slight shift range of the Raman spectra, i.e., from 2697 cm^{-1} to 2700 cm^{-1}. Beside that, in Fig. 4b, a significant 2D peak shift range is observed for NL device, from 2686 cm^{-1} up to 2704 cm^{-1}.

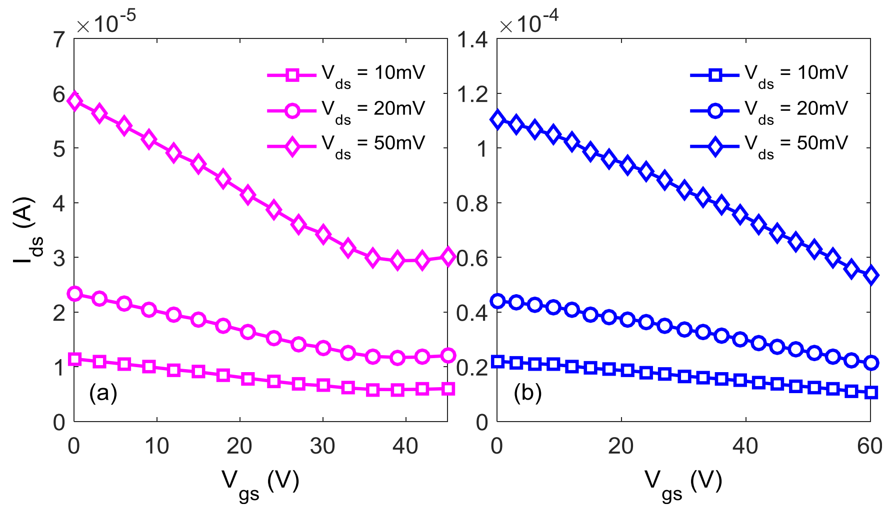

Fig. 3. Transfer characteristics of the (a) NL device and (b) L device.

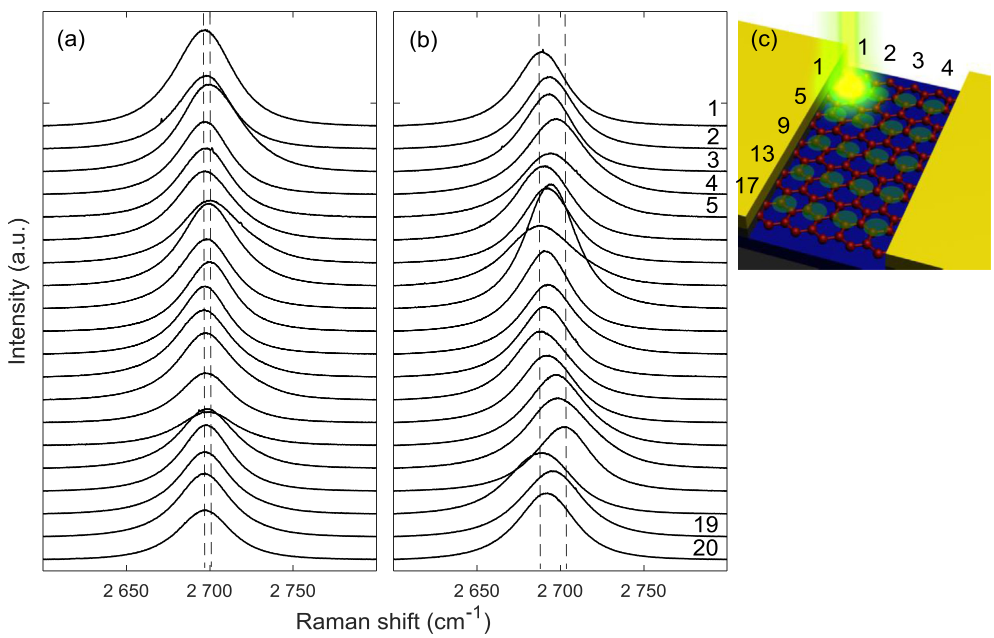

Fig. 4. Raman spectra for (a) L and (b) NL devices showing the 2D peak shift evolution. (c) 3D schematic representation of the Raman measurements performed according to 4 × 5 grid over the graphene ribbon area.

The results shown in Fig. 4 are comparable with those obtained when applying a back-gate voltage [10,11]. Indeed, the Raman shift was found proportional to the applied gate voltage, also, proportional to the carrier density and thus the Fermi level. Nevertheless, in the case of Fig. 4b, we get a large range of the 2D shift without any bias. In the absence of a back-gate voltage, the carrier density presents localized different values over the ribbon area, which implies a non-uniform carrier density.

Otherwise, it was reported [7,14] that the quality of the graphene plays a decisive role in the electrical response of graphene devices.

The positions of the 2D peak can be associated to proper values of the carrier density [10], in this way, the spectra positions plateau for L device correspond approximately to $1–2 \times 10^{13}$ cm^{-2} carrier density. These results reveal that the Au/Ti/p-type-monolayer-graphene junction is ohmic for a graphene carrier's concentration of $1–2 \times 10^{13}$ cm^{-2}. As a result, the linear behavior shown in Fig. 2b is due to one relevant consequence issued from the fabrication process: the fact that the graphene ribbon was highly doped from its environment during the fabrication process. In this case, the work functions of the metal and the graphene are aligned, as a result, the carriers across the barrier easily which makes the contact as ohmic.

For the NL device, the spectra evolution corresponds approximately to a carrier density ranging from 5×10^{12} cm^{-2} to 2×10^{13} cm^{-2}. Therefore, the difference in the 2D peak positions reveals that carrier density is not uniform over the ribbon area. However, the Raman measurements are in agreement with the initial Hall measurements. In the other hand, to explain the NL behavior, the previous work of Landauer el al [18] reported that the transport carrier's concentration along the ribbon (channel) is affected by electrostatic oxide charge density. The total transport carrier's density n_{tot} is expressed as:

$$n_{tot} = n_{ox} + n_{\min}, \quad (1)$$

with n_{ox} is the oxide charge density which is governed by the inhomogeneity of the electrostatic potential.

Consequently, the association of the Equation (1) with the measurements reported in Fig. 4b reveals that two technological parameters are at the origin of the nonlinear behavior. First, the fact that the carrier density is localized in terms of concentration over the ribbon area, second, the contacts are ohmic which implies the existence of a carrier density gradient in the graphene ribbon at the metal boundary.

Shin et al. [13] attributed the nonlinearity in the monolayer graphene ribbon devices to the presence of impurities and active radicals in the graphene, which are source of doping. Therefore, our measurements and results not assess this conclusion. Indeed, the L device measurements attest that we can get a linear behavior for doped graphene ribbon.

4. Conclusion

Two categories of electrical behavior (linear and non-linear output characteristics) in back-gated graphene ribbons are reported. The linear behavior reveals that the Au/Ti/p-type-monolayer-graphene junction is ohmic for a graphene carrier's concentration of $1–2 \times 10^{13}$ cm^{-2}. For graphene ribbon-based structures, the local carrier density along the channel plays a crucial role for the transport properties, so it is of great importance to characterize this in well controlled experiments. The Raman analysis provides solid evidence for the analysis of the electrical behavior of the graphene ribbons. Indeed, the results reveal that the linear behavior is due to a highly doped graphene, while the nonlinear behavior is strongly related to the graphene localized carrier's densities.

Acknowledgements

The authors would like to acknowledge the Action de Recherche Concertée (ARC) “Stresstronics” and “Naturist” projects granted by the Communauté fançaise de Belgique for their financial support. We also acknowledge Wallonia Infrastructure for Nano FABrication (WINFAB) and Wallonia ELectronics and COmmunication MEasurements (WELCOME) for electrical and Raman measurements. The corresponding author would like to express his thankfulness to the MESRS PNE program for supporting his scholarship to the UCL-ICTEAM. Particular thanks to Ferran Urena, P.A. Haddad and B. Huet for devices fabrication.

References

[1] K.S. Novoselov, A.K. Geim, S.V. Morozov, D. Jiang, Y. Zhang, S.V. Dubonos, I.V. Grigorieva, A.A. Firsov, Electric field effect in atomically thin carbon films, Science 306 (2004) 666–669.
[2] F. Schwierz, Graphene transistors, Nat. Nanotechnol. 5 (2010) 487–496.
[3] L. Vicarelli, M.S. Vitiello, D. Coquillat, A. Lombardo, A.C. Ferrari, W. Knap, M. Polini, V. Pellegrini, A. Tredicucci, Graphene field-effect transistors as room-temperature terahertz detectors, Nat. Mater. 11 (2012) 865–871.
[4] S. Srisonphan, Y.S. Jung, H.K. Kim, Metal-oxide–semiconductor field-effect transistor with a vacuum channel, Nat. Nanotechnol. 7 (2012) 504–508.
[5] A. Westlund, M. Winters, I.G. Ivanov, J.U. Hassan, P.-Å. Nilsson, E. Janzén, N. Rorsman, J. Grahn, Graphene self-switching diodes as zero-bias microwave detectors, Appl. Phys. Lett. 106 (2015), 093116.
[6] S. Gilje, S. Han, M. Wang, K.L. Wang, R.B. Kaner, A chemical route to graphene for device applications, Nano Lett. 7 (2007) 3394–3398.
[7] F. Giubileo, A. Di Bartolomeo, The role of contact resistance in graphene field-effect devices, Prog. Surf. Sci. 92 (2017) 143–175.
[8] A.C. Ferrari, D.M. Basko, Raman spectroscopy as a versatile tool for studying the properties of graphene, Nat. Nanotechnol. 8 (2013) 235–246.
[9] R. Beams, L.G. Cançado, L. Novotny, Raman characterization of defects and dopants in graphene, J. Phys. Condens. Matter 27 (2015), 083002.
[10] A. Das, S. Pisana, B. Chakraborty, S. Piscanec, S.K. Saha, U.V. Waghmare, K.S. Novoselov, H.R. Krishnamurthy, A.K. Geim, A.C. Ferrari, A.K. Sood, Monitoring dopants by Raman scattering in an electrochemically top-gated graphene transistor, Nat. Nanotechnol. 3 (2008) 210–215.
[11] C. Stampfer, F. Molitor, D. Graf, K. Ensslin, Raman imaging of doping domains in graphene on SiO_2, Appl. Phys. Lett. 91 (2007), 241907.
[12] P.-H. Wang, F.-Y. Shih, S.-Y. Chen, A.B. Hernandez, P.-H. Ho, L.-Y. Chang, C.-H. Chen, H.-C. Chiu, C.-W. Chen, W.-H. Wang, Demonstration of distinct semiconducting transport characteristics of monolayer graphene functionalized via plasma activation of substrate surfaces, Carbon 93 (2015) 353–360.
[13] Y.J. Shin, K. Gopinadhan, K. Narayanapillai, A. Kalitsov, C.S. Bhatia, H. Yang, Stochastic nonlinear electrical characteristics of graphene, Appl. Phys. Lett. 102 (2013), 033101.
[14] F.A. Chaves, D. Jiménez, A.W. Cummings, S. Roche, Physical model of the contact resistivity of metal-graphene junctions, J. Appl. Phys. 115 (2014), 164513.
[15] J.S. Moon, M. Antcliffe, H.C. Seo, D. Curtis, S. Lin, A. Schmitz, I. Milosavljevic, A.A. Kiselev, R.S. Ross, D.K. Gaskill, P.M. Campbell, R.C. Fitch, K.-M. Lee, P. Asbeck, Ultra-low resistance ohmic contacts in graphene field effect transistors, Appl. Phys. Lett. 100 (2012), 203512.
[16] K.-E. Byun, H.-J. Chung, J. Lee, H. Yang, H. Song, J. Heo, D.H. Seo, S. Park, S.W. Hwang, I.K. Yoo, K. Kim, Graphene for true ohmic contact at metal–semiconductor junctions, Nano Lett. 13 (2013) 4001–4005.
[17] S.A. Thiele, J.A. Schaefer, F. Schwierz, Modeling of graphene metal-oxide-semiconductor field-effect transistors with gapless large-area graphene channels, J. Appl. Phys. 107 (2010), 094505.
[18] G.M. Landauer, D. Jiménez, J.L. González, An accurate and verilog-a compatible compact model for graphene field effect transistors, IEEE Trans. Nanotechnol. 13 (2014) 895–904.
[19] I. Meric, M.Y. Han, A.F. Young, B. Ozyilmaz, P. Kim, K.L. Shepard, Current saturation in zero-bandgap, top gated graphene field effect transistor, Nat. Nanotechnol. 3 (2008) 654–659.
[20] D.L. John, L.C. Castro, D.L. Pulfrey, Quantum capacitance in nanoscale device modeling, J. Appl. Phys. 96 (2004) 5180.
[21] T. Fang, A. Konar, H. Xing, D. Jena, Carrier statistics and Quantum capacitance of graphene sheets and ribbons, Appl. Phys. Lett. 91 (2007), 092109.
[22] L. Vicarelli, S.J. Heerema, C. Dekker, H.W. Zandbergen, Controlling defects in graphene for optimizing the electrical properties of graphene nanodevices, ACS Nano 4 (2015) 3428–3435.